



Study on grinding performance during ultrasonic vibration-assisted grinding ultra-high strength steels

Ming Han¹ · Yi Tang² · Wenfeng Ding¹ · Junshuai Zhao¹ · Biao Zhao¹ · Guoliang Liu³ · Mingming Deng³ · Menglan Tang³

Received: 27 April 2023 / Accepted: 10 August 2023 / Published online: 22 August 2023
© The Author(s), under exclusive licence to Springer-Verlag London Ltd., part of Springer Nature 2023

Abstract

Super high-strength steel has an important demand in manufacturing key components inside gear transmission systems of heavy-duty helicopter owing to its superior comprehensive mechanical property. However, the high-performance machining of super high-strength steel is confronted with great challenges owing to the high cutting force, serious tool wear, and impoverished machining quality. Comparative trials in grinding ultra-high strength steel under conventional grinding (CG) and ultrasonic vibration-assisted grinding (UVAG) processes were conducted with white alumina (WA) and microcrystalline alumina (MA) wheels. Grinding performances, including grinding forces, force ratio, ground surface quality, and abrasive wheel morphologies, were discussed in detail. Experimental results show that the separation property between wheels and workpiece in UVAG process contributes to alter the material removal process, reducing the chip clogging and adhesion. In addition, the micro-fracture of abrasive grains can effectively improve the self-sharpening ability of abrasive wheels. UVAG possesses a shorter grinding scratch owing to the ultrasonic vibration than that of CG, which is beneficial to improve machining quality under the same wheel. Meanwhile, in comparison of WA wheels, MA wheels have the narrower grinding marks and better surface quality, which is due to the sharp edges produced by its higher strength, toughness, and excellent self-sharpening.

Keywords Ultrasonic vibration-assisted grinding · Ultra-high strength steel · White alumina wheel · Microcrystalline alumina wheel · Grinding performance

1 Introduction

Recently, ultra-high strength steels have attracted an increase attention to prepare high-performance gears in helicopter transmission system to confront the complex and severe environment, owing to their superior mechanical properties (e.g., high hardness and high toughness) [1, 3]. Grinding as the final and crucial manufacturing processes was widely used to ensure the machining accuracy and surface integrity

[4, 5]. However, the ultra-high strength steels after quenched treatments have the dispersed reinforced particles, leading to the difficult-to-machine properties on the near-layer surface of workpiece [6, 7]. Moreover, the large grinding force and temperature usually appear in the conventional grinding (CG) process, and then serious abrasive wheel wear and impoverished grinding surface quality are also inevitable owing to the dispersed reinforcements on workpiece surface [8, 12]. In this case, it is very significant to lessen the grinding force and temperature and thus improve the wear-resistance performance of alumina wheel and grinding quality through employing a new grinding technology.

Ultrasonic vibration assisted grinding (UVAG) was usually applied to improve the machinability of materials and machining quality by changing the relative motion relationship between grinding grains and workpiece [13, 18]. Meanwhile, the different material removal mechanisms and grinding performance related to various steel materials were investigated at home and abroad [19, 22].

✉ Wenfeng Ding
dingwf2000@vip.163.com

¹ National Key Laboratory of Science and Technology On Helicopter Transmission, Nanjing University of Aeronautics and Astronautics, Nanjing 210016, China

² Communication University of China, Nanjing College of Art and Design, Nanjing 210016, China

³ AECC Zhongchuan Transmission Machinery Co., Ltd, Changsha 410200, China

Tawakoli et al. [23, 24] carried out contrastive experiments on the influence of ultrasonic vibration in dry grinding soft steels. They revealed that the utilization of ultrasonic vibration could avoid the heat damage on the metal surface, accelerate the ratio of F_t/F_n , and diminish the grinding forces. Ding et al. [25] studied the wear process of WA wheels while grinding of AISI9310 steels under UVAG and CG processes and found that UVAG could prolong the stable wear stage by 23.07% and reduce the surface roughness at a stable level. In addition, the abrasive cutting edge was easy to break or pull-out, which deteriorated the machining ability of the abrasive wheel and ground surface quality [26, 28]. Similar, Chen et al. [29, 30] found that UVAG could obtain the better surface roughness during machining C45 steel than that of CG. Meanwhile, the surface running-in stage of UVAG process was short, and it has better load-bearing performance in steady state. Qiu et al. [31] found that the high frequency and discontinuous contact between abrasive particles and workpiece under UVAG condition could promote the generation of abrasive micro-cracks and improve the self-sharpening of grinding wheels. In this case, the high grinding surface integrity could be obtained. Abhimanyu et al. [32, 33] found that the ultrasonic vibration could avoid the plastic damage of the machined surface and improve the surface integrity under dry grinding. Amir et al. [34] reported that the employment of ultrasonic vibrations into CG processes of X210Cr12 steel could avoid the damages of ground surface. However, the researches on the grinding performance of ultra-high strength steels after applying ultrasonic

vibrations were rarely carried out and the associated material removal mechanism lacked in-depth study.

In this work, the UVAG and CG comparative trials with ultra-high strength steels using white alumina (WA) and microcrystalline alumina (MA) wheels are conducted, aiming at revealing the grinding performance and material removal mechanism. After introducing experimental details and methods, the grinding performances, in terms of grinding forces and force ratio, grinding quality, and abrasive wheel morphology, are analyzed in detail. Finally, the conclusions are summarized in last section.

2 Experimental details and methods

2.1 Experimental equipment

The equipment utilized in this experiment is a BLOHM Profimat MT-408 precision surface grinding machine, which boasts exceptional cooling capabilities with a flow rate of 90 L/min and pressure of 1.5 MPa, as depicted in Fig. 1. Here, the as-developed ultrasonic vibration system is erected on the worktable (Fig. 1a). The ultrasonic transducer receives the high-frequency electrical signal of the ultrasonic generator and converts it into ultrasonic vibration. Then, the ultrasonic vibration is amplified by the horn and transmitted to the tool chuck, which makes the workpiece produce ultrasonic vibration. Figure 1b shows the details of the workpiece clamping. Two workpieces are fixed on the ultrasonic welding head, and the workpieces

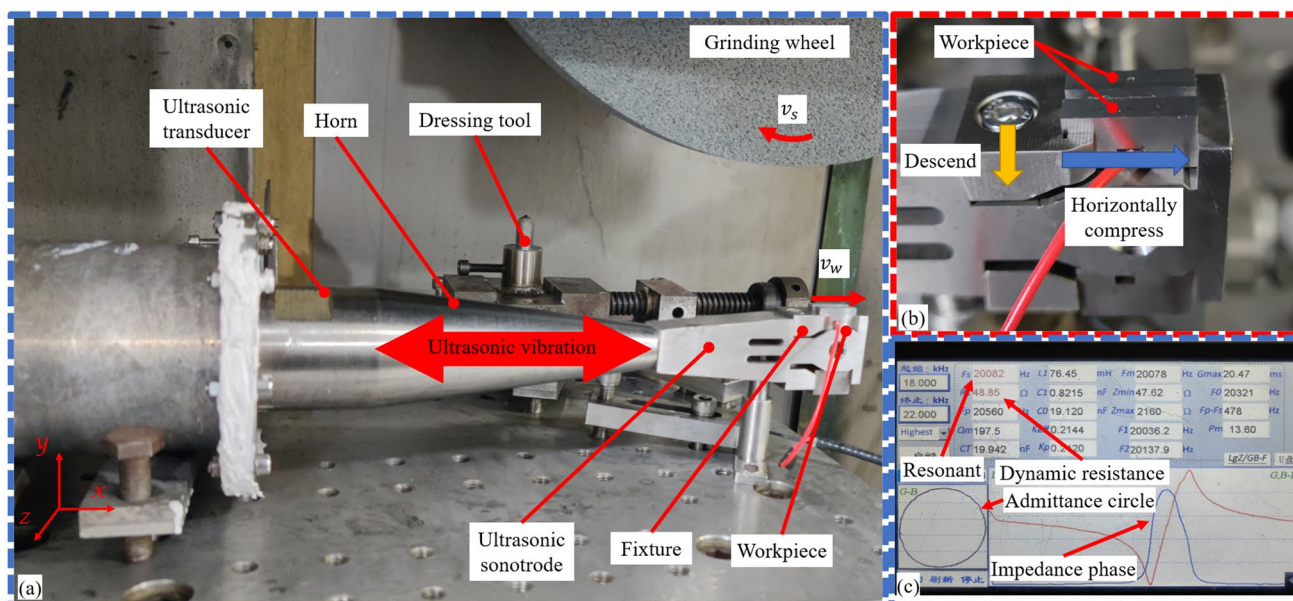


Fig. 1 Grinding experimental equipment: (a) arrangement of ultrasonic vibration system, (b) workpiece clamping details at the end of the device, (c) resonance information of ultrasonic system.

are separated by thin metal blocks in the middle to ensure that the abrasive wheel can grind one workpiece at a time. Figure 1c displays the resonance frequency and admittance circle information of the workpiece clamped by the ultrasonic device, with a stabilized ultrasonic vibration frequency of 20.0 kHz. A laser doppler vibrometer was utilized to measure the unloaded workpiece’s vibration frequency and amplitude, with a fixed sampling frequency of 480 kHz. The real-time FFT analysis conducted with Quick SA software indicates that, at a power output of 25% and a vibration frequency of 19.6 kHz, the workpiece is capable of generating a stable ultrasonic amplitude (A) measuring 3 μm . The abrasive wheels used in this experiment are WA and MA, which are suitable for grinding hardened steel materials including ultra-high strength steel. The abrasive wheel models are WA80J6V45m/s and

MA80J6V45m/s. The abrasive size of the abrasive wheel is about 160–200 μm . The wheel diameter d_s is 400 mm, and the axial width b_s is 20 mm. Figure 2a and b shows the two kinds of abrasive wheels and their surface morphologies. Other details of the experiment are listed in Table 1.

The used workpiece material is the ultra-high strength steel after the carburizing treatment (15Cr14Co12Mo5Ni), and Tables 2 and 3 show the main chemical composition and mechanical properties of the materials. Here, the workpiece is preprocessed using wire cutting method with a dimension of 20 mm (in length) \times 5 mm (in height) \times 16 mm (in width). Prior to the grinding experiment, the grinding surface is machined to a high surface quality the ground surface roughness R_a ($\leq 0.8 \mu\text{m}$), and the clamped surface is machined to the surface roughness R_a ($\leq 1.6 \mu\text{m}$) to ensure the transmission effect.

Fig. 2 Surface topography of WA wheel (a) and MA wheel (b)

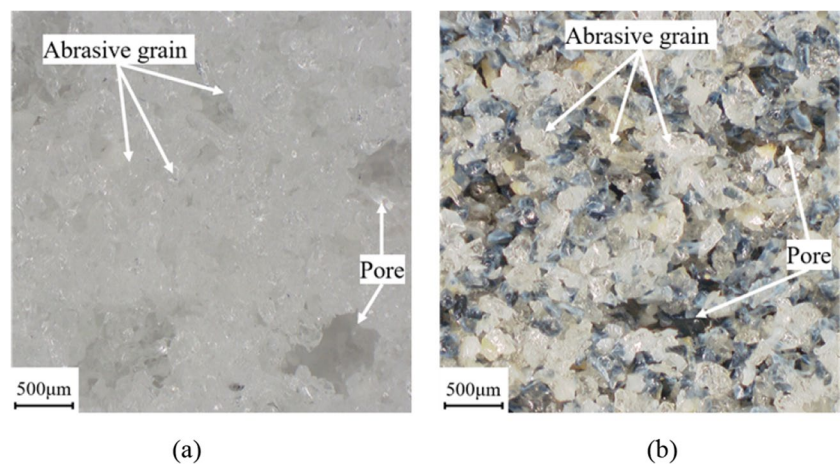


Table 1 Grinding parameters

Parameters	Values
Machine tool	High-speed surface grinder (Blohm Profimat MT-408)
Grinding mode	Down grinding
Abrasive wheel	WA80F6V45M and MA80F6V45M 400 mm (excircle) \times 127 mm (hole) \times 20 mm (width)
Workpiece	Ultra-high strength steel (15Cr14Co12Mo5Ni) 20 mm (length) \times 5 mm (width) \times 16 mm (height)
Dressing condition	Dressing speed $v_{ds} = 20 \text{ m/s}$ Dresser longitudinal feed speed $v_{dw} = 50 \text{ mm/min}$ Wheel radial feed depth $a_{pd} = 0.015 \text{ mm}$ Total dressing amount $a_d = 0.2 \text{ mm}$
Grinding speed v_s	10–30 m/s
Workpiece speed v_w	0.6–2.5 m/min
Depth of cut a_p	20–110 μm
Coolant	5% emulsified water, 90 L/min, pressure at 1.5 MPa

Table 2 Chemical composition of materials

Element	C	Cr	Co	Mo	V	Ni
Component/%	0.15	12.5	11.0	4.50	0.70	2.20

Table 3 Properties of materials

Workpiece material	Tensile strength σ (MPa)	Hardness (HRC)	Yield strength σ (MPa)	Fracture toughness K_{IC} (MPa·m ^{1/2})
15Cr14Co-12Mo5Ni	1780	66	1380	75

2.2 Experimental process

High pressure air is used for continuous cooling during the operation of the ultrasonic device. Single point diamond corrector is used for dressing of grinding wheel before grinding, and the dressing parameters of the abrasive wheel are listed in Table 1. Grinding experiment coolant is 5% emulsified water of 1.5 MPa. The grinding force was collected by Kistler 9253B 3-channel piezoelectric force meter, amplified by Kistler 5080A charge amplifier, and the data were read and processed in DynoWare software. In addition, the collected original signal is low-pass filtered and then analyzed to ensure the reliability of grinding force signals. By averaging the data, the final grinding force was calculated. After this experiment, workpieces were cleaned with anhydrous ethanol, coated

with desiccant, and stored in the dry condition for further analysis. The workpiece grinding R_a was measured by the Mahr M2 perthometer (cut length: 0.8 mm), and the surface profile was obtained by optical microscopy (HIROX KH-7700) and confocal microscopy (Sensofar S neox 3D). The surface microstructure of abrasive wheel was characterized by scanning electron microscope (SEM, Quanta200).

2.3 Analysis of tangential ultrasonic vibration assisted grinding process

As shown in Fig. 3a, the motion process of tangential UVAG consists of three parts: the feed movement of the table v_w , the circular rotation of the abrasive wheel v_s and the frequency produced by the ultrasonic device f , and the amplitude of vibration A . In the grinding process, chips are produced by the slippery rubbing-plowing-chip formation between the feeding workpiece and the rotating alumina grains on the alumina wheel. UVAG makes the opposing motion relationship between alumina grains and workpiece more sophisticated because of the high frequency vibration brought by ultrasound, and the process of grinding and chip generation is changed. The equations for the trajectory of the alumina particles of CG and UVAG are

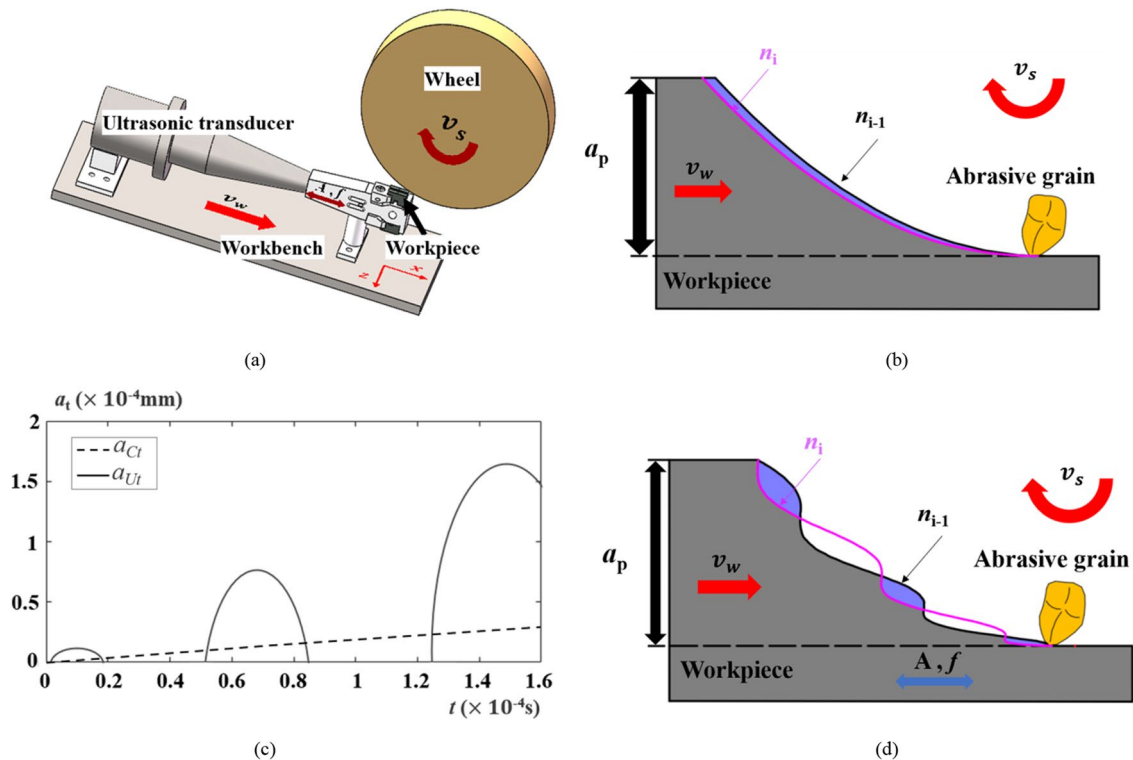


Fig. 3 Comparison between CG and UVAG: (a) relative motion relationship, (b) CG abrasive grain trajectory relationship, (c) variation of cutting depth of single abrasive grains, (d) UVAG abrasive grain trajectory relationship

$$\begin{cases} x_{CG} = -v_{\omega}t - \frac{d_s}{2}\sin(\omega_s t) \\ y_{CG} = -\frac{d_s}{2}\cos(\omega_s t) \end{cases} \quad (1)$$

$$\begin{cases} x_{UVAG} = -v_{\omega}t - \frac{d_s}{2}\sin(\omega_s t) + A\sin(\omega t + \varphi_0) \\ y_{UVAG} = -\frac{d_s}{2}\cos(\omega_s t) \end{cases}, \quad (2)$$

where ω and t are ultrasonic vibration angular frequency and time, respectively, $\omega = 2\pi f$; ω_s is the angular velocity of the alumina wheel, $\omega_s = 2v_s/d_s$, d_s is the wheel radius; φ_0 denotes the initial phase of ultrasonic vibration.

According to $f=19.6$ kHz and $A=3$ μm set in the experimental details, taking $v_s=20$ m/s, $v_w=1.5$ m/min, $a_p=50$ μm substituted into Eqs. 1 and 2, and taking the spacing of adjacent grinding grains on the abrasive wheel as 1 mm, the trajectories of two adjacent grinding grains during CG and UVAG grinding can be obtained by simulation (Fig. 3b and d). Among them, the path lengths of CG and UVAG single wear particles in the grinding zone are, respectively:

$$l_{CG} = \left(\frac{v_s + v_w}{v_s}\right)\sqrt{a_p d_s} \quad (3)$$

$$l_{UVAG} = \left(\frac{v_s + v_w}{v_s} + \frac{4Af}{v_s}\right)\sqrt{a_p d_s} \quad (4)$$

If the CG abrasive chip is simplified into a triangle, the depth of cut of a single grain of CG and UVAG at any point in time t within the grinding arc can be expressed as [18, 35]:

$$a_{Ct} = \frac{\lambda v_{\omega}}{v_s} \sin(\omega_s t) \quad (5)$$

$$a_{Ut} = \frac{d_s}{2} - \frac{d_s \cos \omega_s t'}{2 \cos \omega_s t} \quad (6)$$

where λ is continuous cutting and grinding edge spacing; t' is the time for the previous abrasive grain to move to the corresponding position, the time for the previous abrasive grain to move to the corresponding position:

$$v_{\omega}t' + A \sin \omega t' + \frac{d_s}{2} \sin \omega t' = v_{\omega}\left(t + \frac{\lambda}{v_s}\right) + A \sin \omega\left(t + \frac{\lambda}{v_s}\right) + \frac{d_s}{2} \cos \omega_s t' \cdot \tan \omega_s t \quad (7)$$

Bringing the established parameters into Eqs. 5 and 6 yields the CG and UVAG single abrasive depth of cut versus time shown in Fig. 3a. Figure 3b and d shows the grinding trajectories of the arc surface and the n_{i-1} th particle left by the n_i th abrasive particle in the CG and UVAG processes, respectively. Figure 3c shows the time-varying curves of the cutting depth of a single alumina particle a_{Ct} and a_{Ut} under the CG and UVAG condition. Combined with Fig. 3b–d, it can be seen although the depth of cut in UVAG is several

times that of CG when the alumina grain is cutting into the workpiece, intermittent cutting and impact effect of UVAG’s abrasive grains shortens the cutting length and enhances the cutting depth. This process reduces the friction between alumina grains and workpiece, shortening the stage ratio of chip formations. As a result, more grinding force is utilized for material removal instead of being converted into heat due to frictions. Besides, the self-sharpening of alumina abrasive particles will also be promoted. Thus, keeping the abrasive cutting edge sharp makes it easier to cut into the workpiece surface [36]. From the perspective of alumina grinding wheels, the impact will subject the alumina grains to high instantaneous forces due to the high hardness of ultra-high strength steel. If the hardness and toughness of the alumina grains are not enough, the grains may break in large pieces and fall off excessively during the impact process, accelerating the wear of the grinding wheel and reducing the machining efficiency.

3 Results and discussion

3.1 Grinding force and force ratio

The important parameters of grinding force as characterization of grinding process are one of the main research objects in the grinding process, and its magnitude has a significant influence on the alumina wheel life, abrasive wheel wear, and the quality of the machined surface. The study of grinding forces and force ratio is a prerequisite for further revealing the grinding mechanism, rationalizing the various physical phenomena in the grinding process, and selecting appropriate machining parameters.

Figure 4 shows the comparison of grinding forces between WA and MA abrasive wheel under CG and UVAG. The change trend of grinding force of WA abrasive wheel is the same as that of MA abrasive wheel, and ultrasonic vibration can effectively lower the normal grinding force of two kinds of abrasive wheel, but the reduction ratio is different under different working conditions. A rapid reduction and gradual smooth trends of F_n and F_t can be observed as v_s ranges from 10 m/s to 30 m/s, and UVAG significantly reduces F_n that replication decreases with the increase of v_s , compared with CG. Here, v_w and a_p are set at 1.5 m/min and 50 μm , respectively. When v_s gradually improves in range of 10–20 m/s, compared with the CG, the F_n reductions of the WA and MA grinding wheels are 5.9–19.4% and 31.0–15.0% under the UVAG condition, respectively. When the v_s is 25 m/s and 30 m/s, the F_n reductions of the WA and MA wheel are 9.6–4.5% and 14.5–8.3% under the UVAG condition. This is because as v_s increases, the number of vibrations of the workpiece decreases during the time when a single alumina grain passes through the grinding contact

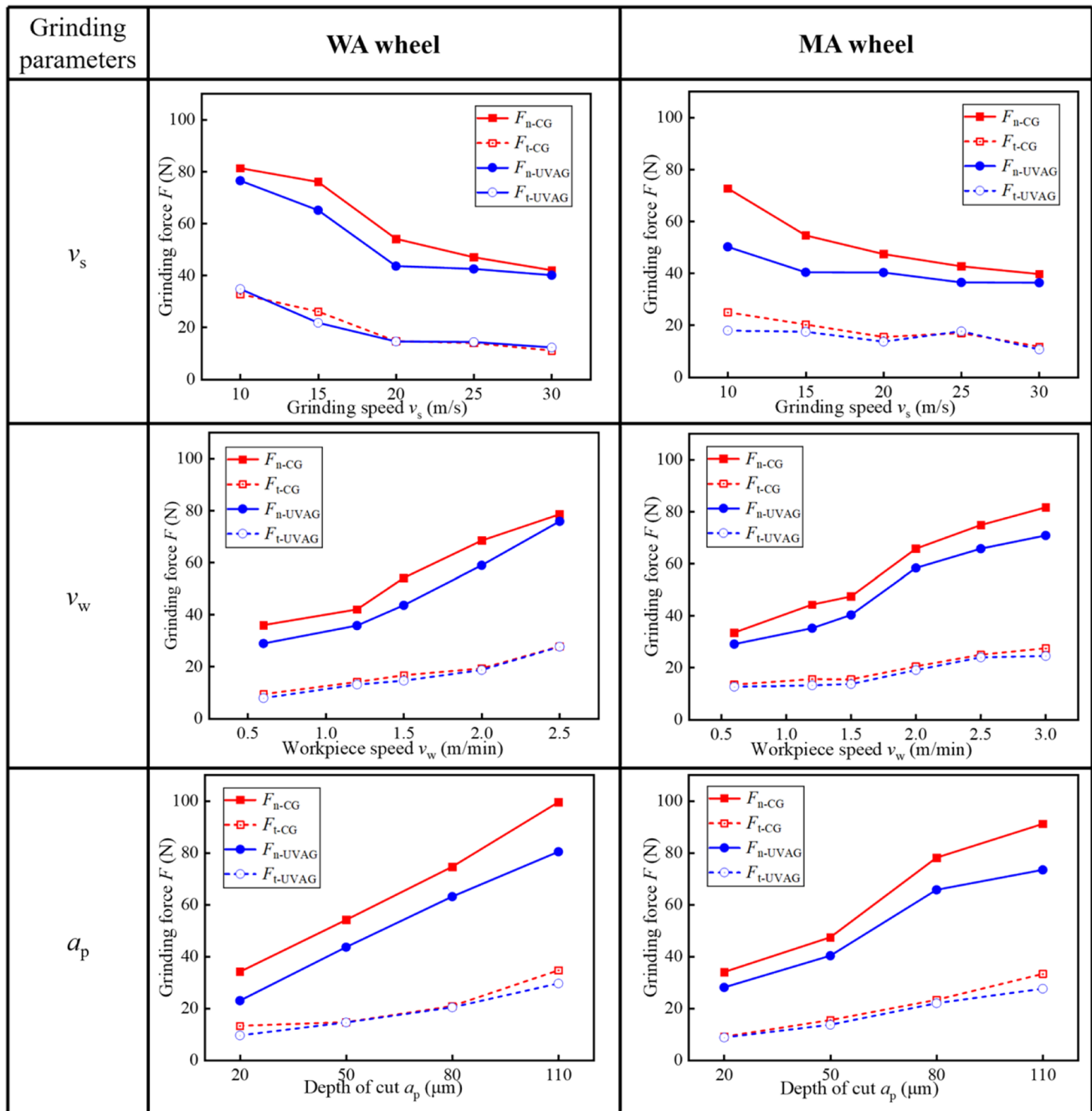


Fig. 4 Effect of grinding parameters on grinding forces under various grinding types

area, the UVAG effect is weakened, and the reduction of the grinding force is reduced.

The normal F_n and tangential F_t grinding force of both WA and MA wheels show an increasing trend as v_w ranges from 0.6 m/min to 2.5 m/min. Under CG conditions, the F_n of MA is always lower than that of WA, the F_t of MA is slightly higher than that of WA at low feed speed, and its grinding force enhances slowly with the enhancement of feed speed and is gradually lower than that of WA.

The F_n of WA and MA wheels increased from 36.0–33.5 N to 78.5–74.8 N, respectively, and the F_t increased from 9.4–10.1 N to 27.8–25.0 N, respectively. Under the condition of UVAG, the normal grinding force of WA and MA wheels increased from 28.9–29.1 N to 75.8–65.7 N respectively, and the tangential grinding force increased from 7.9–11.2 N to 27.7–24.0 N, respectively. Within the experimental parameters, the reduction amplitude under UVAG condition normal F_n grinding force on MA grinding wheel is relatively

stable, but when the v_w more than 1.5 m/min, the reduction amplitude for WA grinding wheel decreases sharply. When v_w increases in range of 0.6–1.5 m/min, the reduction amplitude of ultrasonic vibration for the grinding force in the grinding process of WA is 19.1–14.7%; when v_w is 2 m/min and 2.5 m/min, it is 13.1% and 3.4%, but for the reduction of MA, the value position is between 20.5–12.2%. This is due to the high brittleness and poor toughness of WA in the process of ultrasonic vibration. With the increase of v_w , the instantaneous grinding force of a single abrasive particle under ultrasonic vibration is larger, resulting in the weakening of grinding force reduction effect.

With the increase of a_p , the reduction amplitude of normal F_n grinding force of UVAG on WA wheel jumps up and down, while the reduction amplitude of normal grinding force on MA wheel decreases first and then increases. Under CG conditions, as a_p ranges from 20 μm to 110 μm , the F_n of WA and MA wheels increased from 34.1–34.0 N to 95.5–91.1 N, respectively, and the Ft increased from 13.3–9.1 N to 34.7–33.3 N, respectively. Under the condition of UVAG, the normal grinding force of WA and MA wheels increased from 23.0–28.1 N to 80.4–73.4 N, respectively, and the tangential grinding force increased from 9.6–8.8 N to 29.6–27.6 N, respectively. With the increase of a_p , the reduction amplitude of normal F_n grinding force of UVAG on WA wheel jumps up and down, while the reduction amplitude of normal grinding force on MA wheel decreases first and then step-up. When a_p rises from 20 μm to 110 μm , the normal F_n grinding force reduction range of the WA is 32.6–19.2%, while F_n reduction range of the MA is first from 17.4% to 15.0%, at 20 μm and 50 μm , then rise to 19.4% at 110 μm . This is because when a_p is small, the grinding arc length is short, the auxiliary effect of ultrasonic vibration is weakened, and the reduction amplitude of grinding force is small. While a_p is too large, the impact force brought by ultrasonic vibration will also increase, which will lead to increased wear of WA, the grinding force increases, and the reduction amplitude of MA is greater than that of WA because of the grinding micro-edge produced by micro-crushing.

3.2 Surface quality

Grinding surface roughness and surface topography (such as marks or defects) are usually the most important parameters to evaluate grinding surface quality. Figure 5 shows the changes of surface roughness of WA and MA wheels after CG and UVAG under different machining parameters. In order to reduce the data error, the abrasive wheel is trimmed before grinding and then measured according to the grinding parameters after two strokes on the material surface. Five measuring points are collected under each group of grinding parameters to take the average value. The changing trend of surface roughness is with machining parameters. Under CG

and UVAG conditions, R_a of MA is much higher than that of WA. This is because MA abrasive wheel is wear-resistant and produces some highly exposed abrasive particles after correction. In the two wear strokes before the machining test, the highly exposed abrasive particles are not completely worn out, resulting in deeper wear marks in the grinding process. On the other hand, because of the high brittleness and poor toughness of the WA abrasive wheel, the high exposure abrasive particles are worn and broken in the wear stroke, resulting in a consistent wear mark height and a small roughness value.

The variation trend of R_a is with v_s that the surface roughness of the two alumina wheels first lessens and then step-up, while v_s rises from 15 m/s to 30 m/s. When v_s increases from 15 m/s to 20 m/s, under CG condition, R_a of WA and MA wheels decreases from 0.389–0.522 μm to 0.253–0.406 μm , respectively, and as v_s rises to 30 m/s, R_a of both increased to 0.358–0.46 μm . With the enhancement of v_s , the thickness of undeformed chips of individual alumina particles decreases and R_a decreases. As v_s continues to rise, the grinding force becomes smaller, while the grinding temperature rises at high speeds. In addition, the super-hard surface of ultra-high-strength steel will make the initial stage of alumina wheel wear intensify and increase the fragmentation of alumina grains, and the above combined effects reduce the quality of the grinding surface.

With the increase of v_w from 0.6 m/min to 2.5 m/min (Fig. 5b), R_a of WA and MA wheels increases gradually. Although the roughness of most UVAG is slightly smaller than that of CG, the surface roughness of UVAG of WA and MA wheels is larger than that of CG when v_w is 0.6 m/min. This is because tangential ultrasonic vibration produces an instantaneous displacement in the direction of v_w , which makes the actual feed speed of the workpiece greater than the set 0.6 m/min, and R_a increases. With the enhancement of a_p from 20 μm to 110 μm (Fig. 5c), the surface roughness of WA and MA wheels increases slowly, which decreases from 0.231–0.298 μm to 0.369–0.440 μm , respectively, under CG, and from 0.217–0.305 μm to 0.341–0.451 μm , respectively, under UVAG. In the case, with the increase of a_p , the depth of abrasive cutting into the workpiece surface increases, the thickness of grinding force and undeformed chip increases, the cutting process of abrasive particles between cutting into and out of the workpiece becomes more complex, and the surface quality becomes worse. On the other hand, ultrasonic vibration shortens the cut-in and cut-out period of wear particles, forms small debris rapidly, and reduces the grinding force, which ensures the grinding surface quality and reduces the roughness value. In the range of experimental parameters, the grinding surface roughness obtained by ultrasonic grinding of WA abrasive wheels and abrasive MA wheels are better than that of CG, which proves

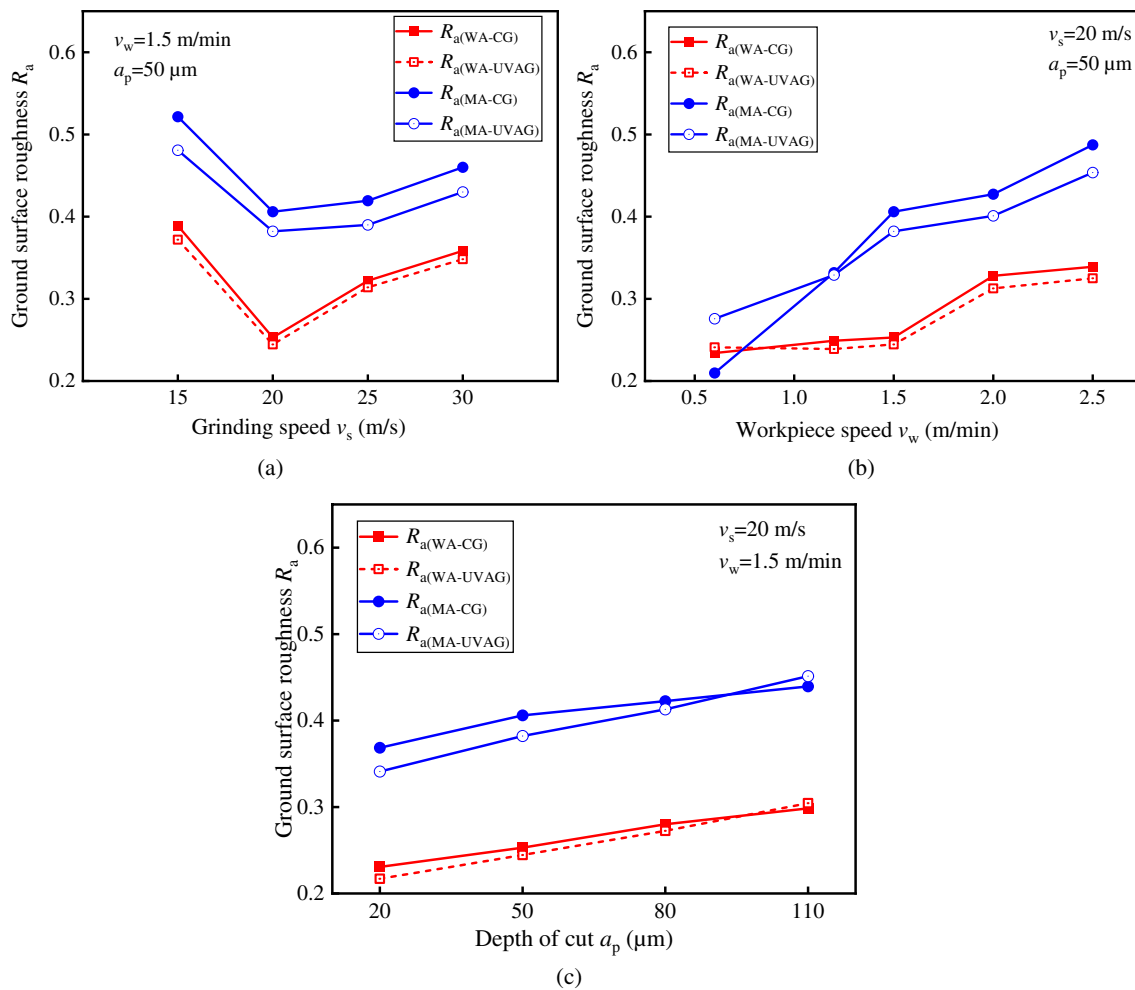


Fig. 5 Influence of grinding parameters v_w (a), v_s (b), and a_p (c) on ground surface roughness R_a

that UVAG can indeed enhance the grinding surface aspect of ultra-high strength steel.

Figure 6 shows the three-dimensional surface topography of WA wheel and MA wheel after conventional grinding and ultrasonic grinding when the machining parameter is $v_s = 20$ m/s, $v_w = 1.5$ m/min, and $a_p = 50$ μ m. Compared with the three-dimensional profile view of WA and MA abrasive wheel, the grinding surface of WA is wider, and the grinding surface of MA wheel is narrow. Compared with the two-dimensional plane photos, the grinding surface of WA abrasive wheel is more obvious; compared with the cross-sectional profile of the grinding surface of WA and MA abrasive wheel, we can see that the grinding surface of WA has a wide profile trough; on the contrary, the trough is sharp and protruding. This well validates the above inference that the WA abrasive wheel has high abrasive brittleness and poor toughness, which results in the wear fracture of high exposed abrasive particles in the wear stroke.

Compared with the plane view of the grinding surface, the wear mark of the grinding surface of the WA abrasive

wheel is more obvious, the wear mark of the ordinary grinding surface is longer, and the wear mark of the ultrasonic grinding surface is short and difficult to distinguish. Combined with the three-dimensional topography of the grinding surface and the cross-sectional profile curve, it can be seen the obvious wear mark on the workpiece surface of WA abrasive wheel is owing to the wide wear mark, while the wear mark of MA abrasive wheel is narrow and deep. This is same as the above assumption that the WA sanding wheel has high brittleness and poor toughness, and abrasive particles with high exposure wear and fracture during wear and tear. Comparing the three-dimensional surface topography of CG and UVAG, it can be seen the wear marks of the two kinds of abrasive wheels under UG conditions are long and continuous, while the wear marks under UVAG conditions are discontinuous and shorter. This is because ultrasonic vibration breaks the long grinding arc, the impact cutting trace of the previous wear particle will be cut away by the next wear particle, and only part of the grinding length remains on the grinding topography.

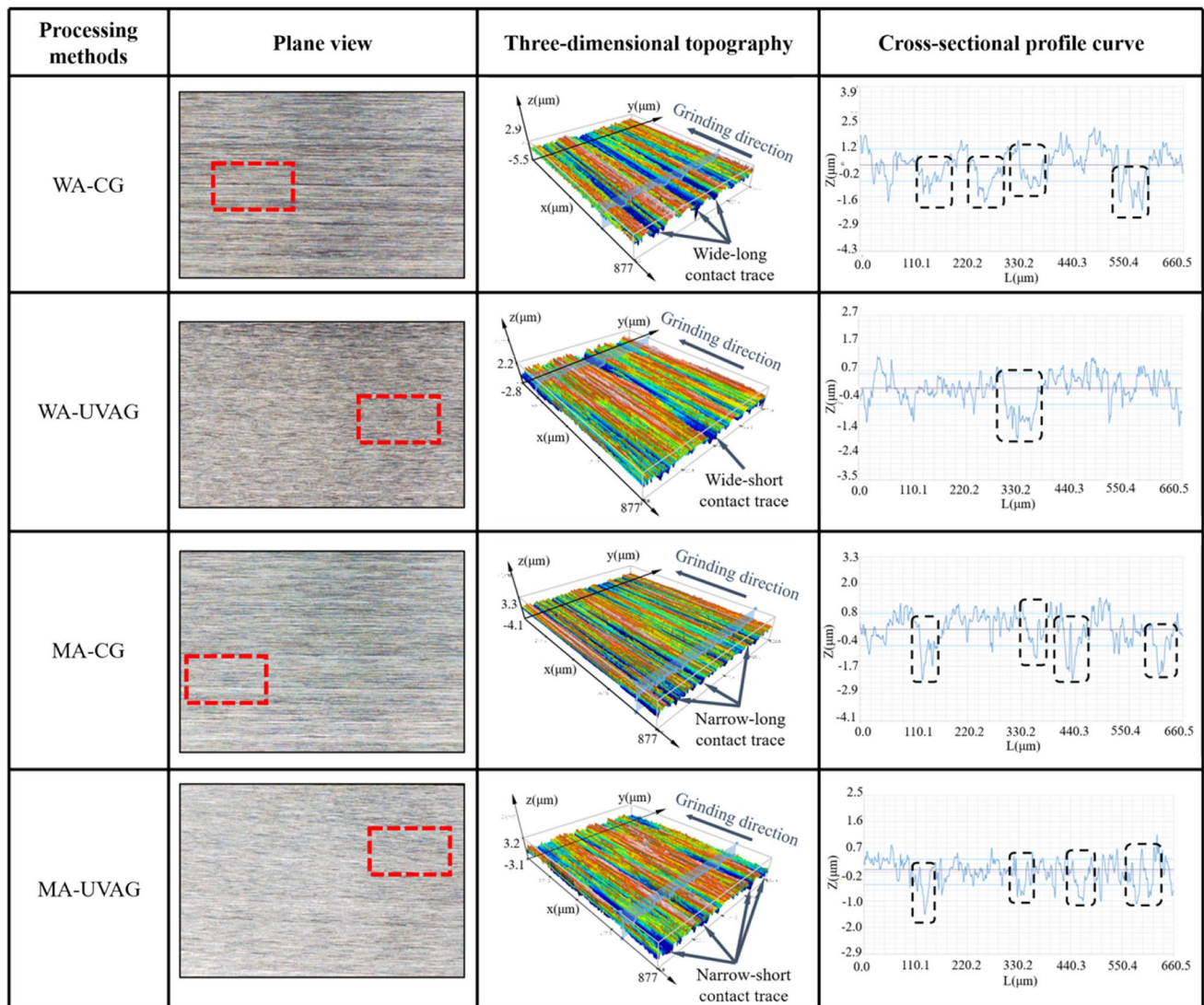


Fig. 6 Grinding surface topography with $v_s = 20$ m/s, $v_w = 1.5$ m/min, and $a_p = 50$ μ m

The peak groove height of WA-CG machined surface is 1.6 μ m and 2.1 μ m, that of WA-UG machined surface is 1.4 μ m and 1.8 μ m, that of MA-CG machined surface is 1.4 μ m and 2.3 μ m, and that of MA-UG machined surface is 1.2 μ m and 2.1 μ m. Comparing the four groups of data, we can see that the peak difference of grooves on the machined surface of WA and MA wheels is similar, but the larger difference in roughness value in Fig. 6 is due to the narrow and deep wear marks on the machined surface of MA wheels. In the calculation of the arithmetic average deviation of the profile, a larger R_a value will be obtained because of the larger absolute value of the longitudinal coordinates from each point to the midline. The peak value of groove height of UVAG is lower than that of CG because under the impact trajectory, the oscillation of grinding track leads to the appearance of crowns and discrowns on the

contour curvature. At the crown, the surface in the UVAG grinding direction is smoother than that in CG. Therefore, the improvement of the peak groove height and R_a of the workpiece in the grinding direction is due to the alternating fluctuation of the surface profile curve along cross section direction [36].

3.3 Abrasive wheel morphology

The morphology of abrasive wheel after grinding material is a significant parameter to analyze the grinding performance of abrasive wheel to material, and it has a very considerable influence on the metal surface. For better observing the surface morphology of WA and MA wheels after CG and UVG, the abrasive wheel surface of ultra-high strength steel after

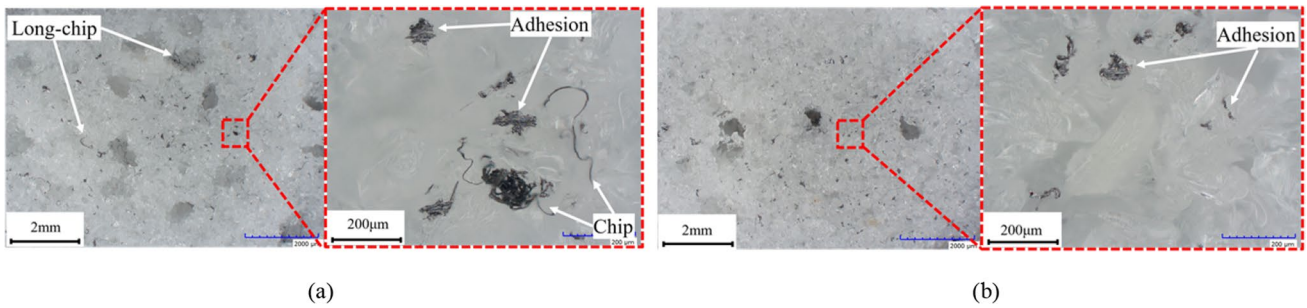


Fig. 7 Surface morphology of the WA wheel after grinding under CG (a) and UVAG (b) conditions

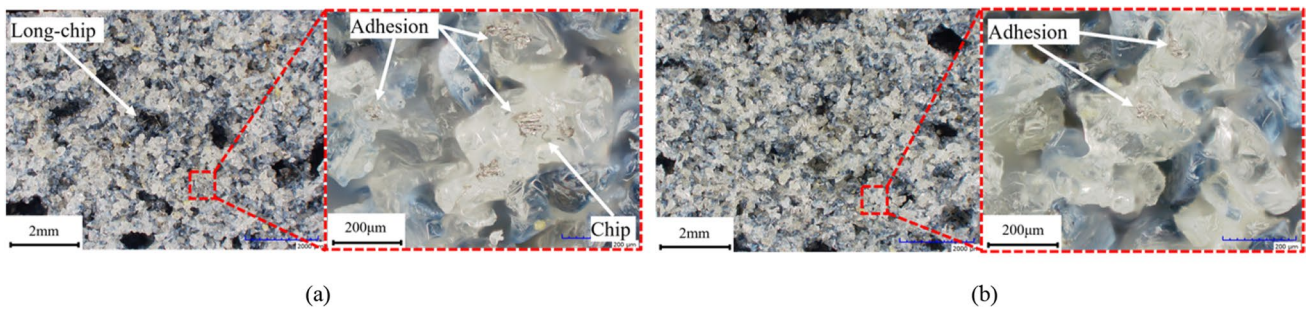


Fig. 8 Surface morphology of the MA wheel after grinding under CG (a) and UVAG (b) conditions

eight strokes was selected and the processing parameter was $v_s = 20$ m/s, $v_w = 1.5$ m/min, and $a_p = 50$ μ m.

As shown in Figs. 7 and 8, the pores of WA and MA wheels include elongated wear debris following CG processes, with large adhesion fragments present on the worn particles. Notably, long strip debris adheres conspicuously to WA abrasive particles but is not observed on MA abrasive wheel. This is due to the smooth cutting edge of abrasive particles during WA grinding, which results in a large grinding force and high temperature. As a result, it is easy for debris to form and weld onto the abrasive particles. After the abrasive wheel grinds the workpiece, the wear debris from welding will combine with new long wear debris to form a mass of debris at the lower right corner

of Fig. 7a, which will significantly impact the quality of metal surface in subsequent processing. After ultrasonic grinding of WA and MA wheels, as depicted in Figs. 7b and 8b, the stomata of alumina wheels appear relatively clean with only a few small debris entering, while patchy debris adheres to the surface without any strip debris observed. However, unlike ultrasonic vibration-assisted grinding of general hardened steel [24], the WA wheel still exhibits significant adhesion of large particles to alumina grains after ultra-high strength steel grinding. This is attributed to the high hardness and wear resistance of ultra-high strength steel itself, as well as the elevated grinding force and heat generated during the process that facilitate chip adherence to alumina grains. Comparing the

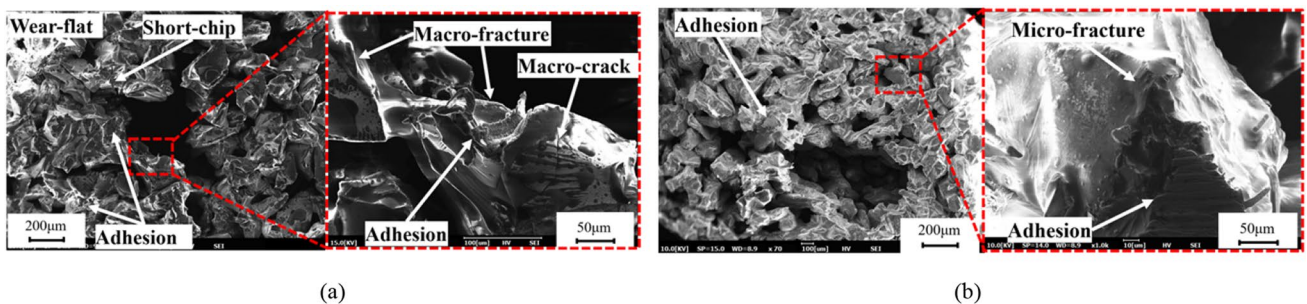


Fig. 9 SEM micro-morphology of the WA (a) and MA (b) wheel after grinding under UVAG conditions

abrasive grains of WA and MA wheels in the figure, it can be observed that the edge angles of MA abrasive cutting edges are more pronounced, while those of WA abrasive cutting edges are less prominent. Additionally, some wear debris adheres to the wear platform.

The morphology of alumina wheels WA and MA after grinding under UVAG conditions is illustrated in Fig. 9. The surface of WA particles exhibits noticeable adhesion of short wear debris, blocky chips, and cracks at the end of abrasive grains, while some abrasive grains form wear platforms (Fig. 9a). After undergoing UVAG process with an MA wheel, the abrasive grains undergo concentrated micro-fragmentation and exhibit minimal adhesion on one side of the cutting edge. Compared to the micro-morphology of abrasive particles after grinding with a WA wheel, the MA wheel produces less adhesion and primarily experiences micro-crushing wear, which is characterized by distinct crushing edges. The UVAG intermittent grinding process improves the wear resistance and self-sharpening properties of the MA wheel, resulting in superior grinding performance when processing harder ultra-high strength steels.

4 Conclusions

In this study, experiments were conducted on ultra-high strength steel using both CG and UVAG techniques with WA and MA grinding wheels. The performance of the two types of wheels was analyzed in detail under different machining processes. Furthermore, the effects of UVAG on corundum wheel performance were examined, including improvements in grinding behavior such as force, morphology, and surface quality. The main conclusions can be drawn:

1. The separation characteristics of UVAG alter the material removal mechanism. In comparison to CG, UVAG exhibits lower grinding force and a stable grinding force ratio. Additionally, during both CG and UVAG processes, the grinding force ratio of MA wheels is smaller than that of WA wheels
2. UVAG contributes to the enhancement of surface quality. In terms of micro-morphology, the groove peak height is lower than that of CG due to UVAG's impact trajectory. Additionally, after grinding with MA wheel, wear marks on the surface are less apparent and grooves are narrower and deeper compared to WA grinding surfaces.
3. The high-frequency interaction between alumina grains and the workpiece interrupts the grinding process, reducing chip clogging adhesion under UVAG conditions. The MA abrasive grain, with its high hardness and toughness, is more likely to produce micro-cutting edges under ultrasonic impact and has better grinding performance than that of WA abrasive grains.

Author contribution Ming Han: experimentation, data curation, and writing the original draft. Yi Tang: data collection. Wenfeng Ding: data collection and manuscript revision. Junshuai Zhao: experimentation and methodology. Biao Zhao: supervision, conceptualization, and methodology. Guoliang Liu: resources. Menglan Tang: funding acquisition. Mingming Deng: funding acquisition.

Funding This work was financially supported by the National Natural Science Foundation of China (Nos. 92160301, 92060203, 52175415, and 52205475), the Science Center for Gas Turbine Project (Nos. P2022-AB-IV-002-001 and P2023-B-IV-003-001), the Natural Science Foundation of Jiangsu Province (No. BK20210295), the Superior Postdoctoral Project of Jiangsu Province (No. 2022ZB215), the National Key Laboratory of Science and Technology on Helicopter Transmission (Nanjing University of Aeronautics and Astronautics) (No. HTL-A-22G12), and the Foundation of Graduate Innovation Center in NUAU (No. XCXJH20220503).

Data availability All data generated or analyzed during this study are included in the present article.

Declarations

Ethics approval and consent to participate The article follows the guidelines of the Committee on Publication Ethics (COPE) and involves no studies on human or animal subjects.

Consent for publication Not applicable.

Competing interests The authors declare no competing interests.

References

1. Waller MD, McIntyre SM, Koudela KL (2020) Composite materials for hybrid aerospace gears. *J Am Helicopter Soc* 65(4):1–11
2. Liang ZQ, Huang DQ, Zhou TF, Li HW, Liu XL (2018) Simulation and experimental research on grinding surface topography of spiral bevel gear. *J Mech Eng* 54(21):183–190
3. Li Q, Xie LY, Song JX, Li HY, Xu GL (2019) Research methods and applications of gear manufacturing process optimization. *Math Probl Eng* 2019:1–17
4. Li C, Wu YQ, Li XL, Ma LJ, Zhang FH, Huang H (2020) Deformation characteristics and surface generation modelling of crack-free grinding of GGG single crystals. *J Mater Process Technol* 279:116577
5. Miao Q, Ding WF, Kuang WJ, Yang CY (2021) Grinding force and surface quality in creep feed profile grinding of turbine blade root of nickel-based superalloy with microcrystalline alumina abrasive wheels. *Chin J Aeronaut* 32(2):576–585
6. Zhao WD, Liu DX, Liu J, Zhang H, Zhang RX, Dong YL, Ye C (2021) The effects of laser-assisted ultrasonic nanocrystal surface modification on the microstructure and mechanical properties of 300M steel. *Adv Eng Mater* 23(3):1–15
7. Dang JQ, Zhang H, An QL, Lian GH, Li YG, Wang HW, Chen M (2021) Surface integrity and wear behavior of 300M steel subjected to ultrasonic surface rolling process. *Surf Coat Technol* 421:127380
8. Wang WX, Salvatore F, Rech J, Li JY (2018) Comprehensive investigation on mechanisms of dry belt grinding on AISI 52100 hardened steel. *Tribol Int* 121:310–320
9. Shao JY, Li KN, Feng YR, Zhang L, Dou Z, Dong DS, Li DS, Xu BC (2023) Effect of lubricants on microstructure and properties

- of metal abrasive tools via wet molding. *Diamond Abrasives Eng* 43(1):59–65
10. Wu BF, Zhao B, Ding WF, Su HH (2021) Investigation of the wear characteristics of microcrystal alumina abrasive wheels during the ultrasonic vibration-assisted grinding of PTMCs. *Wear* 477:203844
 11. Molaie MM, Akbari J, Movahhedy MR (2016) Ultrasonic assisted grinding process with minimum quantity lubrication using oil-based nanofluids. *J Clean Prod* 129:212–222
 12. Pang F, Lei DJ, Wang W (2022) Diamond grinding quality analysis based on controlled grinding depth. *Diamond Abrasives Eng* 43(1):118–125
 13. Wang JJ, Zhang JF, Feng PF, Guo P (2018) Experimental and theoretical investigation on critical cutting force in rotary ultrasonic drilling of brittle materials and composites. *Int J Mech Sci* 135:555–564
 14. Cao Y, Zhu YJ, Ding WF, Qiu YT, Wang LF, Xu JH (2021) Vibration coupling effects and machining behavior of ultrasonic vibration plate device for creep-feed grinding of Inconel 718 nickel-based superalloy. *Chin J Aeronaut* 35(2):332–345
 15. Zheng FF, Kang RK, Dong ZG, Guo J, Liu JT, Zhang JT (2018) A theoretical and experimental investigation on ultrasonic assisted grinding from the single-grain aspect. *Int J Mech Sci* 148:667–675
 16. Zhu XM, Liu Y, Zhang JH, Wang K, Kong HH (2020) Ultrasonic-assisted electrochemical drill-grinding of small holes with high-quality. *J Adv Res* 23:151–161
 17. Zhou WH, Tang JY, Shao W (2020) Modelling of surface texture and parameters matching considering the interaction of multiple rotation cycles in ultrasonic assisted grinding. *Int J Mech Sci* 16:105246
 18. Zhang K, Yin Z, Dai CW, Miao Q, Cheng QH (2022) Undeformed chip thickness characteristics in grain-workpiece contact zone in ultrasonic vibration assisted grinding. *Diamond Abrasives Eng* 42(1):19–23
 19. Yang ZC, Zhu LD, Zhang GX, Ni CB, Lin B (2020) Review of ultrasonic vibration-assisted machining in advanced materials. *Int J Mach Tools Manuf* 156:103594
 20. Shen JY, Dai B, Wu X, Li Y, Hu ZW (2019) Study on the material removal mechanism of glass in single diamond grain grinding with ultrasonic vibration assisted. *Int J Abras Technol* 9(1):60–72
 21. Zahedi A, Tawakoli T, Akbari J (2015) Energy aspects and workpiece surface characteristics in ultrasonic assisted cylindrical grinding of alumina–zirconia ceramics. *Int J Mach Tools Manuf* 90:16–28
 22. Zhu YJ, Ding WF, Rao ZW, Zhao ZC (2019) Self-sharpening ability of monolayer brazed polycrystalline CBN abrasive wheel during high-speed grinding. *Ceram Int* 45(18):24078–24089
 23. Tawakoli T, Azarhoushang B, Rabiey M (2009) Ultrasonic assisted dry grinding of 42CrMo4. *Int J Mach Tools Manuf* 42:883–891
 24. Tawakoli T, Azarhoushang B (2008) Influence of ultrasonic vibrations on dry grinding of soft steel. *Int J Mach Tools Manuf* 48(14):1585–1591
 25. Ding WF, Huang Q, Zhao B, Cao Y, Tang ML, Deng MM, Liu GL, Zhao ZC, Chen QL (2023) Wear characteristics of white corundum abrasive wheel in ultrasonic vibration-assisted grinding of AISI 9310 steel. *Ceram Int* 49:12832–12839
 26. Naskar A, Choudhary A, Paul S (2020) Wear mechanism in high-speed superabrasive grinding of titanium alloy and its effect on surface integrity. *Wear* 462:203475
 27. Li M, Yin JF, Che LB, Ding WF, Xu JH (2022) Influence of alumina abrasive tool wear on ground surface characteristics and corrosion properties of K444 nickel-based superalloy. *Chin J Aeronaut* 35(6):339–351
 28. Wang JW, Yu TY, Ding WF, Fu YC, Bastawros AF (2018) Wear evolution and stress distribution of single CBN superabrasive grain in high-speed grinding. *Precis Eng* 54:70–80
 29. Chen HF, Tang JY (2016) Influence of ultrasonic assisted grinding on Abbott-firestone curve. *Int J Adv Manuf Technol* 86(9–12):2753–2757
 30. Chen HF, Tang JY, Zhou W (2013) An experimental study of the effects of ultrasonic vibration on grinding surface roughness of C45 carbon steel. *Int J Adv Manuf Technol* 68(9–12):2095–2098
 31. Qiu YT, Zhao B, Cao Y, Ding WF, Fu YC, Pu CL (2022) On the grinding performance of alumina wheels in ultrasonic vibration-assisted grinding of hardened GCr15 steel. *Int J Adv Manuf Technol* 120(3–4):1695–1706
 32. Abhimanyu C, Ashwani S, Akash SA, Mohd ZKY, Meghanshu V (2022) Modeling and simulation study of dry ultrasonic vibration-assisted grinding of tool steel with single alumina abrasive grit. *J Manuf Sci Eng* 144(11):111001
 33. Abhimanyu C, Mohd ZKY, Meghanshu V (2021) Grindability study of hard to cut AISI D2 steel upon ultrasonic vibration-assisted dry grinding. *Proc Inst Mech Eng Part E, J Process Mech Eng* 236(3):915–925
 34. Amir A, Mohammad S, Rezvan A, Vahid F (2013) Experimental study on ultrasonic use in dry creep-feed up-grinding of aluminum 7075 and steel X210Cr12. *Int J Precis Eng Manuf* 14:191–198
 35. Huo MY, Zhang JH, Zhang HL (2006) Study on ultrasonic vibration assisted grinding in theory. *Mater Sci Forum* 532–533:773–776
 36. Cao Y, Ding WF, Zhao B, Wen XB, Li SP, Wang JZ (2022) Effect of intermittent cutting behavior on the ultrasonic vibration-assisted grinding performance of Inconel 718 nickel-based superalloy. *Precis Eng* 78:248–260

Publisher's note Springer Nature remains neutral with regard to jurisdictional claims in published maps and institutional affiliations.

Springer Nature or its licensor (e.g. a society or other partner) holds exclusive rights to this article under a publishing agreement with the author(s) or other rightsholder(s); author self-archiving of the accepted manuscript version of this article is solely governed by the terms of such publishing agreement and applicable law.